Functionalization of 3D printed ABS filters with MOF for toxic gas removal

Ismael Pellejero[a*], Fernando Almazán[b], Marta Lafuente[b], Miguel A. Urbiztondo[c], Martin Drobek[d*], Mikhael Bechelany[d*], Anne Julbe[d], Luis M. Gandía[a]

[a]Institute for Advanced Materials and Mathematics (InaMat[2]); Public University of Navarre (UPNA); Edificio Jerónimo de Ayanz, Campus de Arrosadia, 31006 Pamplona-Iruña, Spain.

[b]Nanoscience Institute of Aragon, University of Zaragoza, Department of Chemical & Environmental Engineering, Edificio I+D+i, Campus Río Ebro, C/Mariano Esquillor s/n, 50018 Zaragoza, Spain.

[c]Centro Universitario de la Defensa; Academia General Militar, Ctra. Huesca s/n, 50090 Zaragoza, Spain.

[d]Institut Européen des Membranes, IEM, UMR-5635, ENSCM, CNRS, Univ Montpellier, Place Eugène Bataillon, 34095 Montpellier Cedex 5, France

*Corresponding Authors: ismael.pellejero@unavarra.es, martin.drobek@univ-montp2.fr, mikhael.bechelany@umontpellier.fr

Abstract: Acrylonitrile butadiene styrene (ABS) is one of the most extensively used polymer in 3D printing manufacturing due to its competitive thermal and mechanical properties. Recently, a special attention has been devoted to novel ABS composites featuring extra functionalities e.g. in the area of VOC removal. Herein, we report on a facile protocol for the functionalization of 3D printed ABS filters with a MOF (Metal-Organic Framework) material (ZIF-8) targeting the conception of attractive gas filters. The proposed synthesis strategy consists in low temperature ALD (Atomic Layer Deposition) of ZnO on the ABS grid followed by the hydrothermal conversion of ZnO to ZIF-8, both steps being conducted at 60 °C. In such way, the method enables an effective growth of ZIF-8 without altering the stability of the polymeric ABS support. The as-fabricated ABS/ZIF-8 filters offer a promising adsorption behaviour for dimethyl methylphosphonate (~20.4 mg of DMMP per gram of ZIF-8), thus proving their potential for toxic gas capture applications.

Keywords: ZIF-8; 3D printing; ABS filter; Atomic Layer Deposition; VOCs abatement, gas treatment.

Highlights:

- Robust method for functionalization of 3D printed ABS filters with MOFs
- Low temperature ALD of ZnO and its hydrothermal conversion to ZIF-8
- Attractive VOC adsorption properties of ABS/ZIF-8 composite for air filtration

Graphical Abstract:

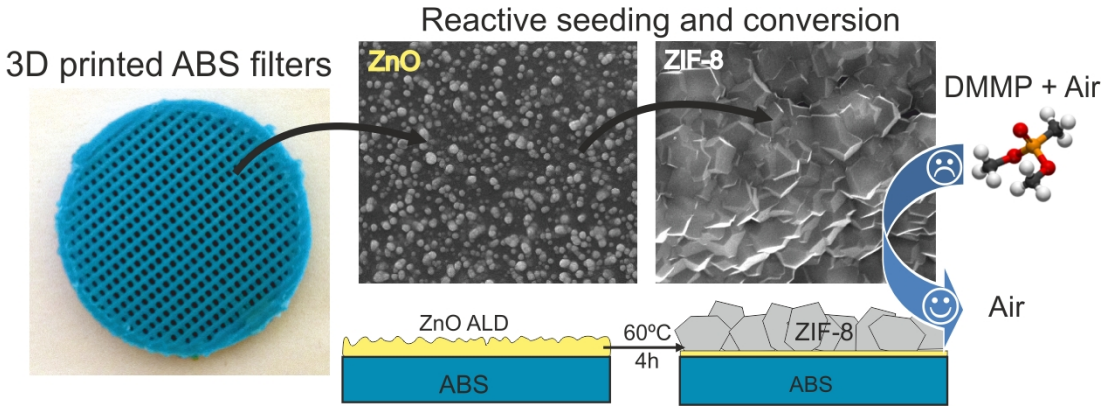

1 Introduction

Additive manufacturing techniques based on 3D printing are nowadays having huge impact on the way the current fabrication methods are changing and adapting [1, 2]. Indeed, these technologies provide attractive fabrication strategies with major competitive advantages, as they are easy-handling and adapted to geometrical complexity and customised designs at low cost. Among the different 3D printing methods the Fused Filament Fabrication (FFF), based on extruding thermoplastic materials, is the most extended one. A typical example of a key material for FFF is ABS (Acrylonitrile Butadiene Styrene) polymer featuring both remarkable chemical and physical stability coupled with easy extrusion. In order to widen the field of ABS applications, huge effort has been made in designing various ABS-composites with tuneable adsorption properties, wettability, good thermal stability and high mechanical strength. Such composites are typically prepared either by addition of the active materials (fillers) in the ABS matrix prior to its fabrication [3-8], or by post-synthesis surface modification/functionalization of the final ABS filter with the selected functional materials [9]. In this work, we propose the surface modification of 3D printed ABS filters with a thin layer of a Metal Organic Framework (MOF) material (here ZIF-8, Zeolitic Imidazolate Framework).

Due to their ultrahigh porosity, large surface areas, structural diversity with versatile micropore sizes, and rich functionalities, MOFs have been developed for multiple applications including gas storage and separation, catalysis and sensing [10-12]. Concerning their synthesis on polymer supports, number of research works have been focused on the development of MOF-polymer composite membranes and filters for either gas [13] or oil/water emulsion separations [14]. Two kinds of membrane designs are typically considered in the literature: *i)* MOF Mixed-Matrix membranes (MMM) where MOF particles are used as fillers incorporated in a polymer matrix [15, 16] or *ii)* supported MOF layers which are grown or deposited on the surface of a prefabricated polymer material [17, 18]. The first design is the most common for 3D printing applications. Typically the pre-synthesized MOF crystals are mixed with a thermoplastic material flowed by an extrusion of the composite (filament shape) in FFF 3D

printer [11, 19, 20], or in the case of stereolithography printing (SLA), MOF crystals are mixed with a photopolymer resin and incorporated to the 3D structure during the curing step [21]. The main drawback of both protocols bears on lowering both the mechanical stability of the composites and the accessibility of the active material flooded in the bulk of the polymer matrix. Hence, the latter design based on material surface modification provides significant advantage over bulk matrix modification. The surface modification approach, often based on MOF secondary growth, requires an optimized support seeding with MOF nanocrystals [22-24]. A uniform seeding could be however very challenging on complex 3D structures and it is thus tricky to growth uniformly a MOF crystal layer on the whole support surface. To overcome this drawback, in this work we applied a synthesis protocol based on "reactive support seeding" involving the deposition of the metal precursor (ZnO) by Atomic Layer Deposition (ALD) [25, 26] and its solvothermal conversion to MOF (ZIF-8) [18]. Based on atom-by-atom reactive deposition mechanism, ALD enables the functionalization of ABS filters with a uniform ZnO layer, thus forming a uniform precursor distribution for homogeneously growing the MOF (ZIF-8) material on the filter. In fact, unlike other deposition techniques such as impregnation, sputtering or CVD, only ALD enables the synthesis of high quality ultrathin films of inorganic materials even on complex 3D structures. This unique ALD capability permits to achieve an excellent grade of metal oxide coverage [27-29] and was thus selected as a technique of choice for the functionalization of the studied ABS filters.

The metal oxide-to-MOF-conversion strategy has been already successfully applied for growing MOFs on flat silicon wafers [25], textile fibers (polypropylene (PP), polybutylene terephthalate (PBT), polyacrylonitrile (PAN) and cotton) [30-33] or alumina membrane supports [34]. In the present work, the reactive seeding by ALD has been used for the first time for the synthesis of MOF functionalized 3D printed structures, targeting their application as active gas filters. To achieve the preparation of such composite materials, the applied synthesis protocol has to warrant MOF growth in aqueous medium (hydrothermal conversion), thus

avoiding the use of organic solvents (often methanol) that could alter the polymer stability and the 3D structure of the filter.

In order to demonstrate the proof of concept for the application of such ABS/ZIF-8 filter systems in air purification, a series of adsorption experiments have been conducted with the composite materials using dimethyl methylphosphonate (DMMP) as a probe gas molecule. The DMMP is a well-known G-series nerve agents simulant, often used to imitate Sarin gas because of its similar chemical structure but much lower toxicity [35]. Due to the exceptional adsorption and reaction capacities of MOFs, many research efforts have been already conducted focusing on their possible application in the capture and/or fast degradation/conversion of toxic agents [36-39]. Hence, the proposed combination of the 3D printed filter with a uniform ZIF-8 layer is expected to be advantageously integrated in such kind of toxic gas capture/elimination systems [40].

2 Materials and Methods

2.1 Fabrication of 3D printed ABS filters.

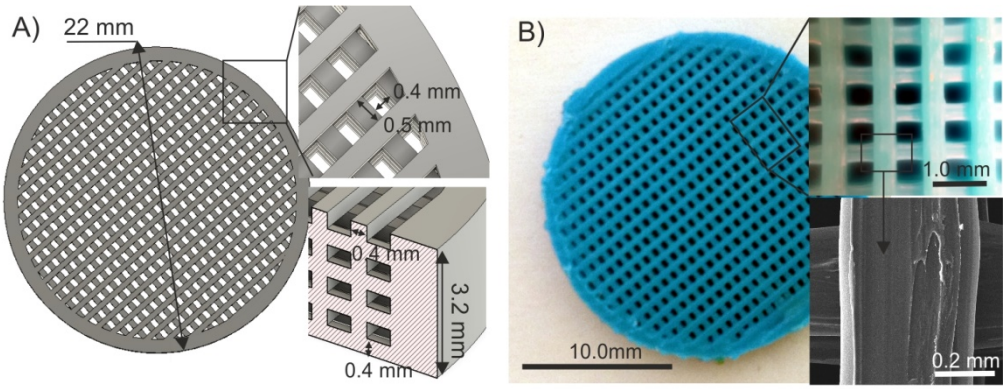

Fig. 1: 3D printed ABS filter. A) CAD design, B) printed filter images.

Series of 3D ABS filters have been fabricated by FFF methodology using ABS (SMARTFIL® ABS Smart Materials 3D) and a desktop 3D printer ZortraxM200 3D printer (extrusion parameters: 235 ºC, 1.75 mm filament, 10 mm·s^{-1}). Fig. 1 shows a typical 3D printed ABS filter with disc geometry (22 mm x 3.2 mm), designed by a computer-aided design software (AutoCAD®). Different mesh dimensions and spacing were tested for selecting the

optimal grid design constituted of perpendicular lines (400 µm x 400 µm) and rectangular openings (400 µm x 500 µm). ZnO by Atomic Layer Deposition

A home-made ALD set-up [41] was used for depositing ZnO layers on both 3D printed ABS filters and companion Si wafer samples (1 mm x 1 mm, polished; <100> oriented). ZnO layers were deposited at two different temperatures (60 °C and 100 °C) using sequential exposure of the metal precursor (diethyl zinc (DEZ), $Zn(CH_2CH_3)_2$, Sigma Aldrich, 95% purity) and deionized water, separated by a purge with dry argon (Ar flow rate of 100 sccm). The deposition protocol was as follows: a) 0.5 s pulse of DEZ, 30 s exposure and 40 s purge with dry Ar; b) 2 s pulse of H_2O, 30 s of exposure, and 40 s purge with dry Ar (*i.e.* total duration ~ 10 h). The selected pulse, exposure and purge times were chosen both to ensure completion of the ALD surface reactions and to prevent any mixing of the reactive species. The measured growth rate of ZnO layer on Si wafers was 0.2 nm per cycle. The thickness (typically in the range 50 nm - 100 nm) and optical characteristics of the deposited layers were analysed by ellipsometry (Semilab GES5E) on flat Si samples.

2.2 ZIF-8 by ZnO conversion

The conversion of ZnO to ZIF-8 was carried out by hydrothermal treatment in a closed pressure vessel (Teflon–lined stainless steel autoclave - 20 ml) containing an aqueous solution of 2-methyl imidazole (2-mIm) (Alfa Aesar, 97% purity). The influence of the main hydrothermal reaction parameters (temperature, reaction time and reactants concentration) was first conducted on flat ZnO-coated Si samples in order to determine the optimal conditions for growing polycrystalline ZIF-8 layers on ABS filters. The 2-mIm concentration was varied fixed at 0.2, 0.5 and 1wt.%, hence in stoichiometric excess compared to the deposited quantity of ZnO. The syntheses were conducted in the temperature range 25-100 °C in a conventional oven. Reaction times were varied from 4 to 24 hours depending on the synthesis temperature. After the hydrothermal treatment, samples were washed with deionized water and dried for 1 h at

60 °C. Optimized ZIF-8 growth conditions were subsequently transferred to 3D printed ABS samples designed for VOCs sorption experiments.

2.3 Sample characterization

Full characterization of the prepared 3D filters was conducted by Field Emission Scanning Electron Microscopy (FESEM), Energy-dispersive X-ray spectroscopy (EDX), X-ray Diffraction (XRD), Thermogravimetric Analysis (TGA), Differential Scanning Calorimetry (DSC) and Fourier Transform Infrared spectroscopy (FTIR). The morphology and homogeneity of the supported ZnO and ZIF-8 on both Si wafers and ABS 3D printed filters were studied at different locations of the samples using field emission scanning electron microscopy (FESEM, Hitachi S-4800 and INSPECT-F50 with Energy-dispersive X-ray spectroscopy (EDX) for elemental analysis. Prior to FESEM observations, the filters were cut with a diamond saw and metalized with palladium by plasma sputtering. Crystalline structures were studied by X-ray diffraction (XRD, D-Max Rigaku, Ru300) using graphite filtered Cu-Kα radiation (X-ray power: 40 kV, 80 mA) and the scanning programme: 2θ = 5-45°; step = 0.03°; time per step = 1s. FTIR spectra were measured on Jasco 4000 equipment with a high throughput monolithic diamond Attenuated Total Reflectance (ATR) accessory. All spectra were recorded by averaging 25 scans in the 4000-400 cm^{-1} range. The DSC spectra were measured using a DSC822e equipment from METTLER TOLEDO with a heating rate of 10 °C·min^{-1} up to 500 °C. Thermogravimetric analyses were performed in air flow (50 mL·min^{-1}) with a heating rate of 5 °C·min^{-1} up to 600 °C (TGAQ5000, TA Instruments). N_2 adsorption-desorption isotherms were obtained with a Micromeritics Gemini V 2380 analyser at 77 K, previously degassed at 100 °C overnight.

2.4 Adsorption studies with DMMP

Adsorption experiments with DMMP (dimethyl methylphosphonate) were carried out by loading the ABS/ZIF-8 filters into the adsorption column (quartz tube $Ø_{int}$ = 22 mm) of a lab-made set-up described in our previous work [42]. Trace-level DMMP vapor atmospheres were

generated by circulating 10 mL·min^{-1} dry N_2 through a calibrated permeation tube (VALCO, permeation rate of 1629.96 ng/min ± 0.71% at 100 ºC) and further analyte dilution was obtained with additional dry N_2 stream until target concentration C_0 = 162 mg·m^{-3} (32 ppmV). A flow of 10 mL·min^{-1} of the DMMP stream (C_0 = 32 ppmV) was circulated in the adsorption column at room temperature and the concentration of the downstream at any time (C_t) was monitored on-line by gas chromatography coupled with mass spectrometer (Shimadzu GCMS-QP2010). To fully characterize the total adsorption capacity and the associated kinetics, experiments were carried out until the outlet concentration (C_t) was equal to the feed concentration (C_0). The adsorbent material was regenerated and reconditioned overnight at 80 ºC under dry N_2 flow (10 mL·min^{-1}).

3 Results and discussion

As already specified in the experimental part, the most important parameters influencing ZIF-8 growth have been investigated first on Si wafers before transferring the synthesis protocol to 3D printed ABS filters. A particular attention has been devoted to the examination of ALD deposition temperature, ZnO layer thickness, concentration of the organic linker, and hydrothermal treatment temperature and duration. All these parameters were selected to fit the chemical, thermal and mechanical stability of the ABS polymer [43]. Indeed, compared to reference studies published in the literature [25, 44, 45] using organic solvents for ZIF-8 layer synthesis (e.g. dimethylformamide and methanol) in this work we focused exclusively on the utilization of water as a solvent for the organic linker. The target was double: *i)* introducing a more environmentally friendly synthesis protocol avoiding application of organic solvents together with minimizing the amounts of reactants (e.g. intrinsically small quantities of organic precursors required for ALD of ZnO) and ii) preservation of the 3D printed filter structure which may be altered by organic solvents under specific reaction conditions.

3.1 ALD of ZnO on 3D printed ABS filters

The stability of ABS filters under ALD conditions has been also investigated in order to identify the possible temperature window for ALD deposition without compromising the pristine filter characteristics. In fact, the temperature and type of organic precursor used for ALD of metal oxides [9] might seriously affect the ABS structure by polymer swelling, deformation or surface damages. Standard ZnO growing procedures by ALD are usually carried out at temperatures ~100 °C or higher depending on the targeted crystalline characteristics and deposition rate. Taking into account the glass transition temperature for ABS (~105 °C), only ALD temperatures below this value are recommended for this kind of support. Indeed, it has been shown that the simple exposure of ABS filters to temperatures ~ 100 °C does not affect their 3D structure. However, under the ALD conditions at 100 °C the filters tend to deform, revealing that the combination of both high temperature and organometallic species (DEZ) can seriously affect the mechanical integrity of the polymeric material (thermochemical effect). This deformation phenomenon was fully avoided by carrying out the ALD of ZnO at ~60 °C, which corresponds to the highest applicable ALD temperature without any alteration of the ABS filter structure. Both optical and SEM observations (Fig. 2A and 2B) confirmed the absence of any filter deformation at 60 °C, although some ZnO clustering was detected on the filter surface at this temperature (Fig. 2B). Nevertheless, a homogeneous coverage of the ABS sample with ZnO was achieved on all samples and confirmed by EDX spectroscopy (results not shown).

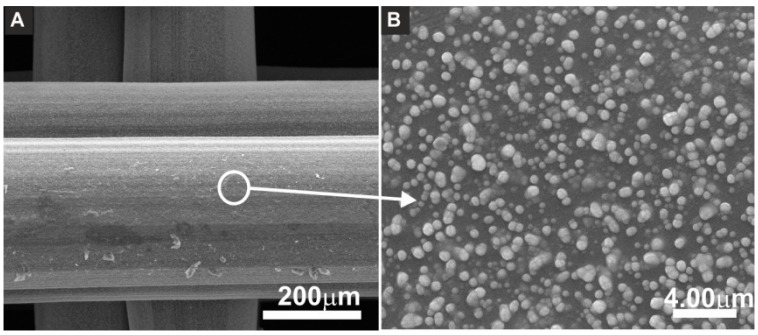

Fig. 2: SEM observation of an ABS filter coated with ZnO (ALD at 60 °C, 50 nm thick ZnO layer measured on Si wafer). A) and B) details of the ZnO-coated ABS surface.

The ALD temperature is a very important parameter impacting the crystallinity, grain size and grain boundaries of the deposited materials [29, 46]. In the present work, ZnO deposition temperature could thus affect the oxide reactivity during its hydrothermal conversion to ZIF-8. Ellipsometry measurements were carried out on Si wafers with 50 nm thick ZnO layers. It has been verified that the thickness of ZnO layer measured on Si wafers corresponds well to the layer thickness deposited on ABS substrates. Indeed, as already observed in our previous studies [47], the ALD rate of ZnO is influenced by the substrate chemistry only during the very first deposition cycles. This initial phenomenon has thus negligible impact on the final layer thickness after the as many as 250 ALD cycles applied to obtain ~ 50 nm thick ZnO layers. The absorption peaks (minimum amplitude Tan Ψ) of ZnO deposited at 60 °C and 100 °C were at 363 nm (3.41 eV) and 370 nm (3.35 eV), respectively, confirming no significant optical differences between the ZnO materials deposited at these two temperatures. Hence, similar crystal sizes and interconnectivity seems to be obtained, independently of the deposition temperature, suggesting similar reactivity for the corresponding layers.

3.2 Synthesis of ZIF-8 by conversion of ZnO ALD layers on Si wafers

Fig. 3 shows FESEM images of ZIF-8 crystals grown by hydrothermal conversion (at different temperatures) of 50 nm thick ZnO layers deposited by ALD on Si wafers at either 60 °C or 100 °C. Whatever the ZnO deposition temperature, similar ZIF-8 crystal sizes and coverage rate were obtained. The lowest deposition temperature (60 °C) has therefore no negative impact on the derived ZIF-8 crystal formation and leads to similar results as the conversion of a ZnO layer deposited at 100 °C. Concerning the temperature for the hydrothermal conversion of ZnO to ZIF-8 in aqueous, a minimum temperature of 60 °C was required in order to ensure sufficient ZIF-8 crystal growth.

When ZnO conversion to ZIF-8 was carried out at lower temperatures (e.g. 25°C), only small and irregular ZIF-8 crystals were formed, leaving the ZnO layer practically intact. Similar results have been obtained even at longer reaction times ≥ 24 h, confirming low ZnO

dissolution/conversion rate at temperatures below 60 °C. Indeed, at 60 °C a nearly full conversion of the 50 nm ZnO layer was achieved within 4 hours, forming ZIF-8 crystals (~1 μm in size) homogeneously spread on the Si wafer surface.

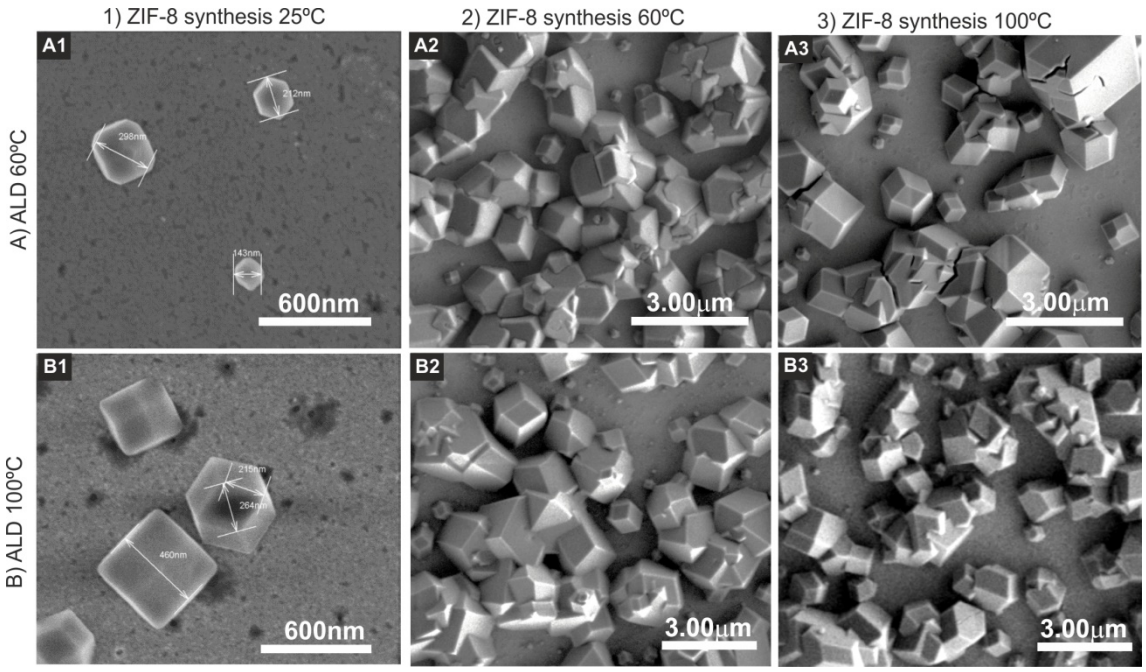

Fig. 3: FESEM images of ZIF-8 crystals obtained by hydrothermal conversion (4 h, 1wt% 2mIm in H_2O): at 1) 25°C, 2) 60 °C and 3) 100 °C, of ALD ZnO layers (50 nm thick) deposited on Si wafers at A) 60 °C and B) 100 °C.

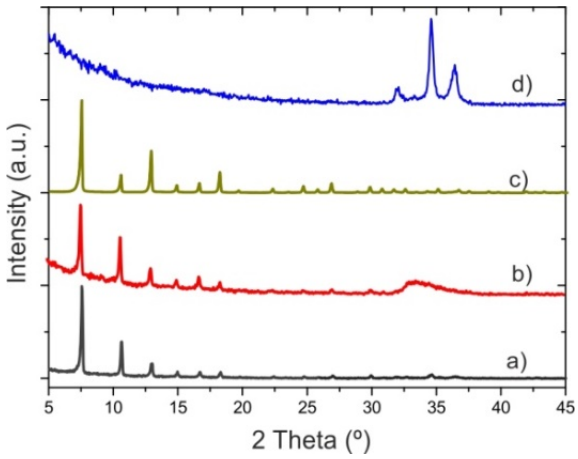

Fig. 4: XRD patterns of ZIF-8 obtained by hydrothermal conversion of ZnO (50nm layer on Si wafers) at: a) 100 °C- 4 h, (ALD at 100 °C) and b) 60 °C - 4h (ALD at 60 °C). The patterns of ZIF-8 crystal c) and ALD of ZnO d) are shown for comparison.

The structural characteristics of the ZIF-8 material obtained by conversion of ZnO ALD layers deposited at either 60 °C or 100 °C have been studied by XRD. As shown on Fig. 4, all

the ZIF-8 characteristic diffraction peaks are well detected, thus confirming the good crystallinity of the formed materials. The large diffraction band in the graph b of Fig. 4 pattern (33-35°, 2θ) was attributed to residual (unconverted) ZnO.

In addition to the temperature for both the ALD of ZnO and the hydrothermal conversion of ZnO to ZIF-8, a series of other synthesis parameters such as ZnO layer thickness and organic linker concentration (2-mIm) has been also investigated. As expected (Fig. 5A), ZnO layers which are ~100 nm thick still partially remained after gentle hydrothermal conditions (4 h-60 °C). Full ZnO conversion required higher temperature (up to 100 °C for the same reaction time). Although none of these reaction conditions allowed obtaining a full and uniform coverage of the Si support with ZIF-8 crystals, improvement could be expected when using longer reaction times at 60 °C in order to slow the crystal growth kinetics. Indeed, the above results demonstrate the direct relation between ZnO layer dissolution and ZIF-8 nucleation/crystal growth. ZIF-8 crystal nucleation should start from ZnO surface by a dissolution mechanism, linker reaction with Zn^{2+} and ZIF-species clustering in basic media. At 100°C, ZIF-8 crystals grow rapidly, consuming the surrounding ZnO and yielding non-uniform support coverage with large ZIF-8 crystals and spaces between them.

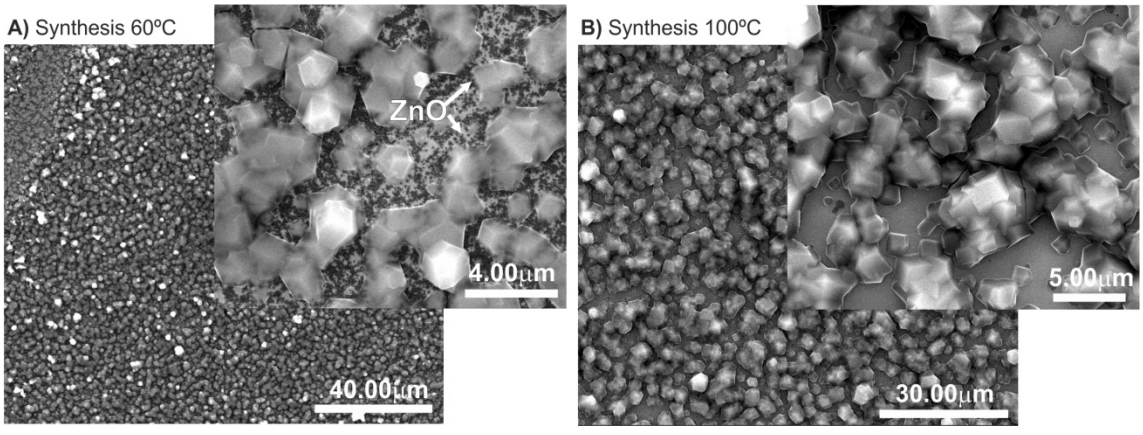

Fig. 5: FESEM images of ZIF-8 crystals obtained by hydrothermal conversion (4 h, 1 wt.% 2mIm in H_2O) at: A) 60 °C and B) 100°C of ALD ZnO layers (100 nm thick) deposited on Si wafers at 60 °C.

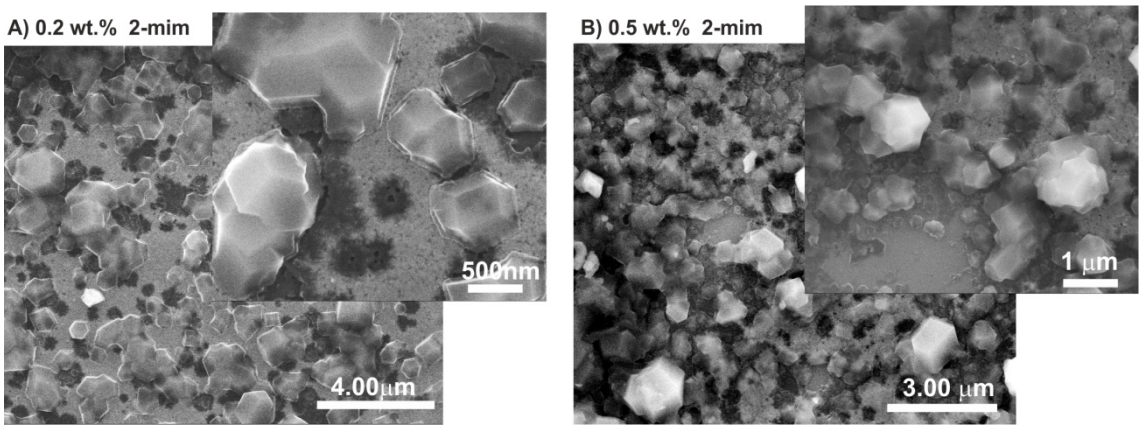

Fig. 6: FESEM images of ZIF-8 crystals obtained by hydrothermal conversion (4 h- 60 °C) with A) 0.2 wt.% 2-mIm; and B) 0.5 wt.% 2-mIm, of ALD ZnO layers (100 nm thick) deposited on Si wafers at 60°C.

Optimal reaction conditions yielding uniform support coverage with connected ZIF-8 crystals should correspond to a compromise between ZnO dissolution and ZIF crystal nucleation and growth rates. The dissolution rate of the ZnO layer is directly related to the pH of the linker solution. Fig. 6 shows the effect of lower concentration of 2-mIm, down to 0.5wt.% (~ pH 10) and 0.2 wt.% (~ pH 9.5), using the same reaction time and temperature (60 °C, 4 h). In comparison with the Fig. 5A, obtained with a higher 2-mIm concentration of 1wt.% (pH 12), the lower pH values are not favourable for a complete dissolution of the ZnO layer and yield heterogeneous growth of ZIF-8 crystals.

3.3 Synthesis of ZIF-8 on ABS filters

As a result of the preliminary investigations on Si wafers, the reaction temperatures for both ALD deposition and solvothermal conversion were fixed at 60 °C for uniform functionalisation of the 3D ABS filters without altering its structure. The hydrothermal conversion of ZnO to ZIF-8 was carried out with 1 wt.% 2-mIm at different reaction times. It is important to note that the low synthesis temperature warrants the possible transfer of the synthesis protocol to other types of polymer materials typically used in FFF process and featuring lower glass transition point.

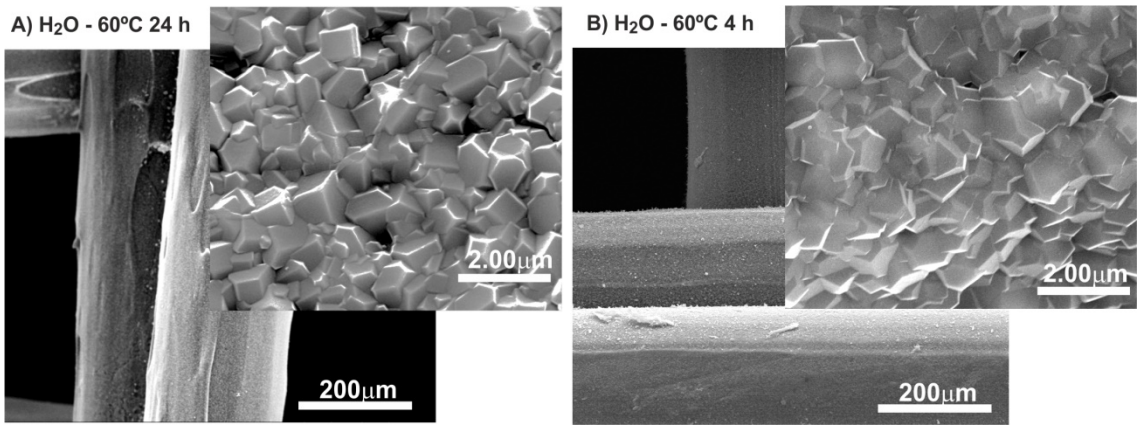

Fig. 7: FESEM images of ZIF-8 grown from ALD-ZnO on the outer surface of ABS filters at A) 60 °C - 24 h and B) 60 °C - 4 h.

As observed on the FESEM images (Fig. 7), the hydrothermal synthesis carried out at 60°C for either 24 h (Fig. 7A) or 4 h (Fig. 7B) led to well intergrown layers homogeneously covering the lines of the filter grid. However, the morphology of MOF crystals/layers grown on ABS support differs from those obtained on Si wafers. We already observed this phenomenon in a previous work focused on the growth of MOFs crystals on polymeric supports (Polyacrylonitrile-PAN) [33] leading to well-intergrown continuous MOFs crystalline layers. Thus MOF crystals intergrowth seems to be better achieved on rough supports rather than on perfectly flat surfaces (Si wafers) featuring no geometrical constrains. This result highlights the asset of the reactive seeding protocol applying ALD to obtain a uniform and high-grade support coverage with MOF layers in comparison with direct MOF synthesis [17, 18] in which full and homogenous coverage are difficult to achieve. To demonstrate the presence of a ZIF-8 layer also on the inner walls of the filter and evaluate its thickness, the MOF modified ABS supports were cut transversally for SEM observations as shown in Fig. 8. It can be clearly seen that, same as on the outer filter walls, homogenous and continuous ZIF-8 crystal layers are also present in the inner areas of the 3D printed filter (Fig. 8B 1-3). Performing the EDS mapping (Fig. 8A 3**)** of the filter cross-section (Zn La1 at 1.02 keV) the ZIF-8 layer thickness was evaluated to be ~ 2 µm. This value is well in the range of the theoretical layer thickness which could be expected by conversion of 50 nm thick ZnO layers (*i.e.* ~ 2.2 µm thick ZIF-8 layer). The lower

values measured for ZIF-8 thickness suggest uncomplete ZnO conversion, as confirmed by XRD analysis (remaining ZnO phase).

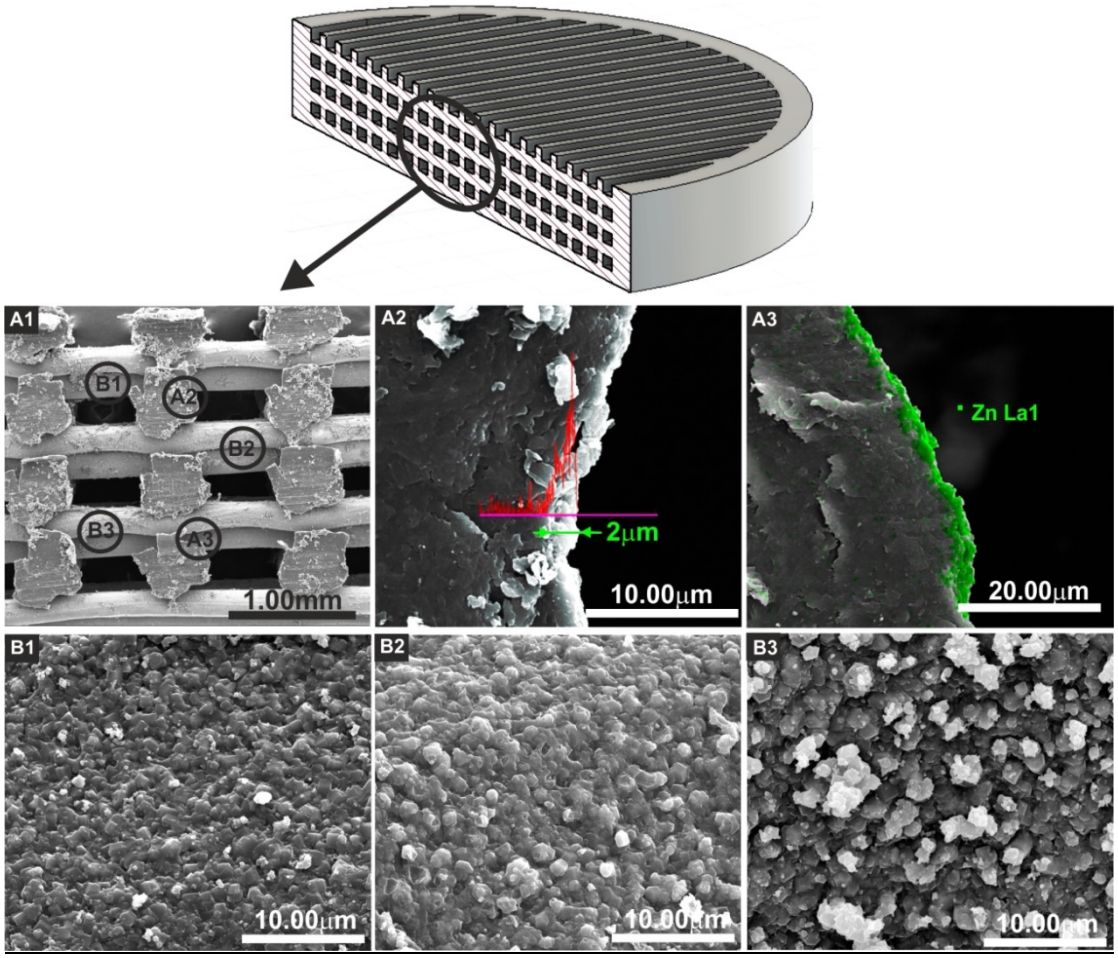

Fig. 8: FESEM cross-section images in different part of an ABS/ZIF-8 filter. A) cross-section, B) slice in the middle of the filter.

It should be underlined that no filter damage was observed even after extended reaction time (24 h). Interestingly, the developed protocol resulted in more uniform layers with better intergrown ZIF-8 crystals than on silicon wafers, thus highlighting the influence of the support and ZnO characteristics on the properties of the derived ZIF-8 layer. In addition, the selected synthesis protocol was found to be very robust as equal amounts of ZIF-8 were grown on filters series having the same architecture (active surface). Typically 2.9 ± 0.6 mg of ZIF-8 were grown on filters with a weight of 520 ± 6 mg (3D architecture described in section 2.1). Due to practical reasons shorter reaction times (4 h) were favoured as the weight of ZIF-8 did not increase significantly after longer reaction times.

From N_2 sorption measurements, the specific surface area of a typical ABS/ZIF-8 filter was evaluated to be 7-8 $m^2 \cdot g^{-1}$, although it was below 1 $m^2 \cdot g^{-1}$ for a bare ABS filter. This increase in S_{BET} could be clearly attributed to the contribution of ZIF-8 material. Considering the quantity of ZIF-8 grown on the surface of the filter (weight increase measurement), a S_{BET} value of ~1300 $m^2 \cdot g^{-1}$ was estimated for the ZIF-8 material alone. In spite of the high error (+20%) associated to this estimated value, it perfectly fits the data reported in the literature for ZIF-8 [48].

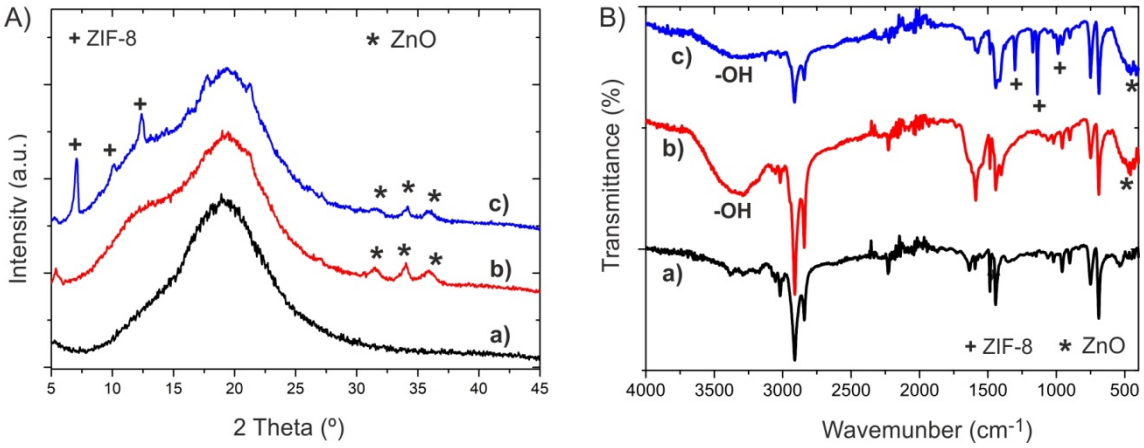

Fig. 9: A) XRD patterns and B) FTIR spectra of ABS filters before and after ZIF-8 synthesis. Graphs a) as-printed ABS filter, b) ABS filter + ALD ZnO at 60 °C, and c) ZIF-8 coated ABS filters (hydrothermal conversion at 60 °C, 4 h).

XRD analyses of the samples confirmed the presence of the main characteristic peaks of both ZIF-8 and ZnO which still remains partially preserved after the ZIF-8 synthesis (Fig. 9). The initial and remaining ZnO layer could serve as a protective shield hindering strong chemical attack of the ABS polymer during the hydrothermal synthesis. Still, when comparing the XRD patterns of a pristine ABS filter and its ZnO-coated analogue (Fig. 9A a) and b), respectively), a slight difference can be observed between 10° and 15°, 2θ, which could be attributed to a small change in the ABS structure during ALD. ABS filters were also subjected to FTIR-ATR analysis (Fig 9B). Bare ABS presents characteristic peaks at 3023 cm^{-1} and 2840–2915 cm^{-1} (C-H, and -CH_3, -CH_2 stretching) together with C-H bending in mono-substituted benzene rings at 755 and 690 cm^{-1} [49, 50]. ABS/ZIF-8 shows bands at 1309 cm^{-1} and 1147 cm^{-1} corresponding to entire ring and aromatic C–N stretching, respectively, while the band at 995 cm^{-1} could be

assigned to C–N bending vibration mode [8, 51] in the 2-mIm ligand. FTIR spectroscopy confirmed that a part of the ZnO remains unreacted (band related to stretching modes of ZnO around 500 cm^{-1} [52] observed for both ABS/ZnO and ABS/ZIF-8 samples), thus corroborating XRD results. The wide band around 3200-3600 cm^{-1} was assigned to surface -OH groups.

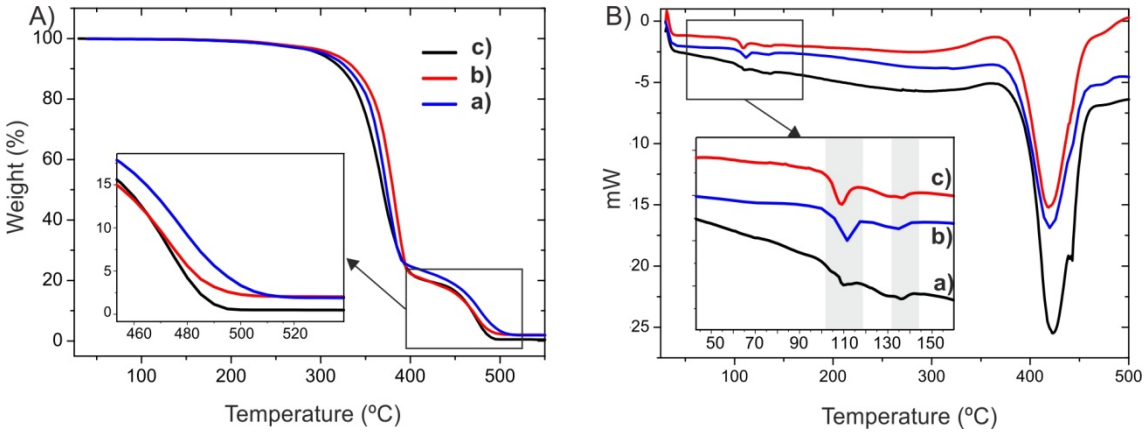

Fig. 10: A) TGA and B) DSC analyses of ABS filters before and after ZIF-8 synthesis. Graphs a) as-printed ABS filter, b) ABS filter + ALD ZnO at 60 °C, and c) ZIF-8 coated ABS filters (hydrothermal conversion at 60 °C, 4 h).

Finally, TGA (in air flow) and DSC analyses were conducted (Fig. 10) in order to determine the stability of ABS matrix before and after MOF synthesis. As observed in Fig. 10A graph a, the total thermal degradation of bare ABS occurs in a wide range of temperatures (275°C - 500°C) with two decomposition steps. The first DTG (Derivative Thermogravimetry) peak at 365°C corresponds to butadiene and styrene, while the second at 475°C is related to monomeric acrylonitrile [53-55]. Comparing the virgin ABS and the support after ALD process and hydrothermal synthesis treatment, no significant difference was observed (DTG peak ±10°C). ZIF-8 degradation was not observed because the range of decomposition temperatures is similar to ABS. DSC analyses (Fig. 10B) confirmed no significant changes in the glass transition temperature after either ABS support exposure to ALD or solvothermal synthesis conditions. Glass transition temperatures (Tg) at 110 °C, and 138°C were attributed to styrene and acrylonitrile, respectively. The main melting temperature peaks at 420 °C were same for all studied samples, thus confirming virtually zero influence of the selected synthesis conditions on the filters stability.

The developed synthesis protocol based on low temperature ALD of ZnO and its hydrothermal conversion to ZIF-8 at low temperature too, permits a total and very uniform coverage of the ABS filter with a high surface area adsorbing material (ZIF-8), without any external deformation or damage of the filter. These 3D printed filters functionalized with an active ZIF-8 layer have been subsequently tested for removing traces of toxic gases from a gas stream by filtration/adsorption.

3.4 Adsorption studies

Dimethyl methylphosphonate (DMMP) was selected as a model compound to test the efficacy of the functionalized 3D ABS/ZIF-8 filters by adsorption in gas phase. Indeed, DMMP is a simulant of the Sarin gas, with much lower toxicity. According to molecular simulation (Fig. S1), the size of the DMMP molecule is 5.17 × 4.24 Å. In a typical experiment the adsorption reactor has been loaded with four ABS/ZIF-8 filters having in total ~12 mg of the ZIF-8 active material deposited on their 3D structure. The efficiency of the filtering system has been then evaluated by flowing through it 32 ppm of DMMP (162 mg·m^{-3}) diluted in N_2 stream at a flow rate of 10 mL·min^{-1}.

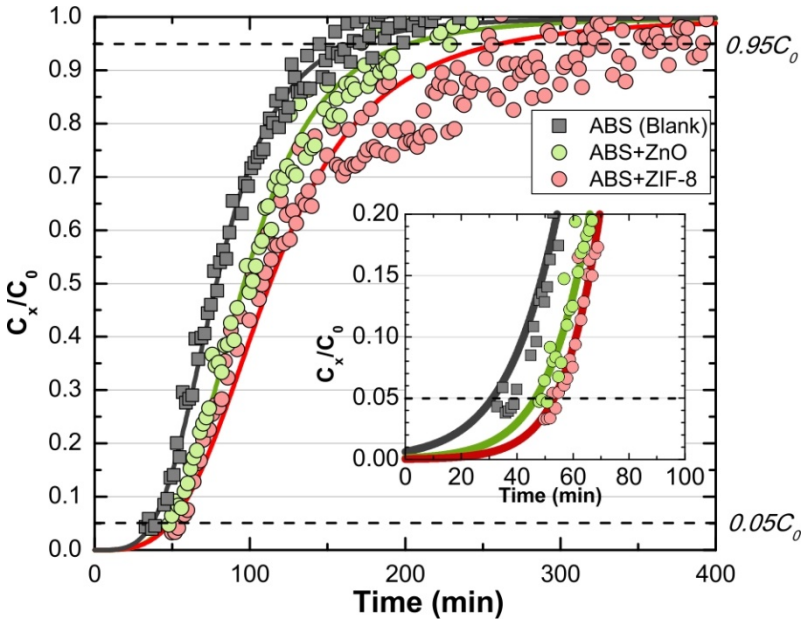

Fig. 11: Adsorption of DMMP by ABS filter (c_{DMMP} 32 ppm), uncoated (blank), ZnO-coated and ZIF-8 coated.

Table 1: Main parameters derived from the breakthrough curves (time, volume and mass of DMMP adsorbed at the breakthrough point (5%) and at the equilibrium point (95%).

Filter	$t_{5\%}$ (min)	$t_{95\%}$ (min)	$V_{5\%}$ (mL)	$V_{95\%}$ (mL)	$m_{5\%}$ (µg)	$m_{95\%}$ (µg)
ABS (Blank)	30.2	163.7	302	1637	48.9	265.1
ABS/ZnO	46.4	202.2	464	2022	75.2	327.5
ABS/ZIF-8	54.8	351.7	548	3518	88.7	569.7

The characteristic breakthrough curves are shown in Fig.11. In spite of its large size, the DMMP molecules is able to diffuse within the ZIF-8 framework because the elastic behavior of ZIF-8 (flipping motion of ligands) allows possible opening of pore apertures up to ~4.2 Å [56]. Different parameters can be determined (Table 1): time $t_{5\%}$, volume $V_{5\%}$ and mass $m_{5\%}$ of analyte adsorbed at the breakthrough point (when outlet concentration C_t is 5% of inlet concentration C_0), and $t_{95\%}$, $V_{95\%}$ and $m_{95\%}$ at the equilibrium point (when C_t and C_0 are nearly identical ~95% of C_0). After subtracting the blank experiment, the mass of DMMP adsorbed by the ABS/ZnO filter ($m_{t95\%\ (ABS/ZnO)}$) was estimated at ~62 µg although it reached ~305 µg for the ABS/ZIF-8 filter (total weight of ZIF-8 $m_{t95\%\ (ABS/ZIF\text{-}8)}$ = 12 mg). With these parameters, the adsorption capacity (W_e) of the filter system (mg of analyte adsorbed per g of adsorbent) was calculated both with and without the effect of the support in order to evidence the activity of the ZIF-8 layer. The total adsorption capacity of the system was W_e = 0.14 mg of DMMP per g of the filter. However, when considering only the ZIF-8 mass (12 mg) and the amount of adsorbed analyte ($m_{t95\%\ (ZIF\text{-}8)}$ = 242 µg), the adsorption capacity of the ZIF-8 layer was $W_{ZIF\text{-}8}$ = 20.4 mg of DMMP per g of ZIF-8. The efficiency of the whole system (ABS/ZIF-8 filters + reactor) calculated as $W_{5\%}$ / $W_{95\%}$ was 15.5%, revealing a high dead volume for the experimental set-up. Removing the contribution of the intrinsic system adsorption (blank experiment), the filters efficiency is ~20%. For the sake of comparison, a set of adsorption experiments has been also conducted with an equivalent amount of ZIF-8 single crystals packed in a bed microconcentrator (Fig. S2). The adsorption equilibrium was determined to be ~ 145 $mg_{DMMP}/g_{ZIF\text{-}8}$. This experimental value has been further crosschecked by adsorption simulation of DMMP inside the ZIF-8 pores (Fig. S3): a comparable value of

~ 170 mg_{DMMP}/g_{ZIF-8} was found at equivalent partial pressure ~ 162 mg of DMMP·m^{-3}. The higher adsorption capacity measured for the ZIF-8 crystals (in comparison with the studied 3D ABS/ZIF-8 filters) is attributed to both higher accessible surface area of individual ZIF-8 crystals and lower bypassing of the gas in the packed bed microconcentrator, though at the expense of a non-negligible and undesirable pressure drop. Hence, an optimum filter architecture offering a good compromise of adsorbent accessibility *vs*. pressure drop should always be found to allow their efficient integration into real air filtration systems [40].

Indeed, both contact efficiency and adsorption capacity of the ZIF-8 could be easily increased by modifying the filter architecture (increasing mesh of the grid), improving filter design (crosslinked-tortuous mesh), adapting filter loading in the system. and/or by modifying the ZIF-8 surface with catalytic species such WO_3, TiO_2 or MoO_2 [57-59] for *in situ* degradation of DMMP. Hence, it is expected that such optimised 3D printed filters functionalised with MOF layers could be advantageously applied in air purification integrated systems for the capture/elimination of VOCs [8, 11, 40] and pesticides [60].

In a wider context, such adsorbing filters could be also implemented with other 3D printed polymers like HIPS (High Impact PolyStyrene), polyamide, polyethylene terephthalate, polycarbonate, polypropylene or PEEK (PolyEther Ether Ketone). They could be advantageously modified also with other MOFs such as MIL-53(Al) [33], UiO-66 (Zr) [37], eventually ZIF-8 with graphene oxide [61] or ordered mesoporous carbons [62], providing that they can be effectively integrated in 3D printed systems and the applied reaction conditions remain compatible with the thermal and chemical stability of the polymer.

4 Conclusions

In this work we present an effective and robust protocol for surface functionalization of 3D printed polymer filters with a uniform layer of a metal organic framework (ZIF-8) by conversion of a metal oxide layer (ZnO) prepared by ALD. The growth of the MOF crystals was carried out by an environment friendly synthesis protocol in aqueous media without any organic

solvent in order to prevent any polymer deformation. ALD temperature was found to be a crucial parameter for the deposition of ZnO layers by ALD on ABS supports and it was feasible at temperatures as low as 60 °C without altering the support architecture. The hydrothermal conversion of the deposited ZnO layers led to uniform layer of well intergrown ZIF-8 crystals on the whole filter surface. DMMP adsorption experiments revealed promising performance for the prepared ABS/ZIF-8 filters (20.35 mg of DMMP per g of ZIF-8) with a system efficiency of 15.5%. Taking into account the robustness of the synthesis protocol (reactive seeding by ALD followed by the hydrothermal conversion of the metal oxide to MOFs), the concept of polymer filter functionalization could be easily implemented to other MOFs and 3D printed supports, providing that the synthesis parameters are compatible with the physico-chemical stability of the FFF polymers. Finally it should be mentioned that, besides of relatively high capital and operational costs of ALD vacuum based technology, the 3D printing and solvothermal conversion of ALD oxide layers do not represent any significant financial or operational bottleneck for process up-scaling. In addition, the possibility of simultaneous ALD on a huge number of substrates, together with the recent development of low temperature processes, roll-to-roll or other special ALD reactors, will certainly enable economically viable ALD coatings on polymeric supports. Such type of 3D printed filters with an active MOF layer could then be possibly implemented in a large variety of environmental applications such as adsorption systems for removing toxic gases or water pollutants, and last but not least also as pre-concentrators or pre-filters in sensing systems.

Conflicts of interest

The authors declare no conflicts of interest.

Acknowledgments

Financial support from Gobierno de Navarra (grants PC052-23) and from the Spanish Ministerio de Ciencia, Innovación y Universidades and the European Regional Development Fund (ERDF/FEDER) (grant RTI2018-096294-B-C31) is gratefully acknowledged. I. P. thanks

Obra Social la Caixa, Fundación Caja Navarra and UPNA for his research contracts in the framework of the programs “Ayudas Postdoctorales” and “Captación Talento”. L. M. G. wishes to thank Banco de Santander and Universidad Pública de Navarra for their financial support under “Programa de Intensificación de la Investigación 2018” initiative. Authors would like to acknowledge the “Servicio de Difracción de Rayos X y Análisis por Fluorescencia del Servicio General de Apoyo a la Investigación-SAI”, Universidad de Zaragoza. The microscopy work has been conducted in the "Laboratorio de Microscopias Avanzadas" at "Instituto de Nanociencia de Aragón - Universidad de Zaragoza". Authors acknowledge the LMA-INA for offering access to their instruments and expertise.

Appendix A. Supplementary Information

Supplementary material related to this article can be found in the online version.

References

[1] A.O. Laplume, B. Petersen, J.M. Pearce, Global value chains from a 3D printing perspective, J. Int. Bus. Stud. 47 (2016) 595-609.

[2] C. Balletti, M. Ballarin, F. Guerra, 3D printing: State of the art and future perspectives, J. Cult. Herit. 26 (2017) 172-182.

[3] M.L. Shofner, K. Lozano, F.J. Rodriguez-Macias, E.V. Barrera, Nanofiber-reinforced polymers prepared by fused deposition modeling, J. Appl. Polym. Sci. 89 (2003) 3081-3090.

[4] L. Jiang, Y.C. Lam, K.C. Tam, T.H. Chua, G.W. Sim, L.S. Ang, Strengthening acrylonitrile-butadiene-styrene (ABS) with nano-sized and micron-sized calcium carbonate, Polymer 46 (2005) 243-252.

[5] H.Y. Ma, L.F. Tong, Z.B. Xu, Z.P. Fang, Synergistic effect of carbon nanotube and clay for improving the flame retardancy of ABS resin, Nanotechnology 18 (2007) 375602.

[6] D.P. Schmitz, T.I. Silva, S. Ramoa, G.M.O. Barra, A. Pegoretti, B.G. Soares, Hybrid composites of ABS with carbonaceous fillers for electromagnetic shielding applications, J. Appl. Polym. Sci. 135 (2018) 46546.

[7] S. Dul, L. Fambri, A. Pegoretti, Filaments Production and Fused Deposition Modelling of ABS/Carbon Nanotubes Composites, Nanomaterials 8 (2018) 49.

[8] M. Bible, M. Sefa, J.A. Fedchak, J. Scherschligt, B. Natarajan, Z. Ahmed, M.R. Hartings, 3D-Printed Acrylonitrile Butadiene Styrene-Metal Organic Framework Composite Materials and Their Gas Storage Properties, 3D Print. Addit. Manuf. 5 (2018) 63-72.

[9] A. Kestila, K. Nordling, V. Miikkulainen, M. Kaipio, T. Tikka, M. Salmi, A. Auer, M. Leskela, M. Ritala, Towards space-grade 3D-printed, ALD-coated small satellite propulsion components for fluidics, Addit. Manuf. 22 (2018) 31-37.

[10] M. Anson, J. Marchese, E. Garis, N. Ochoa, C. Pagliero, ABS copolymer-activated carbon mixed matrix membranes for CO2/CH4 separation, J. Membr. Sci. 243 (2004) 19-28.

[11] M.C. Kreider, M. Sefa, J.A. Fedchak, J. Scherschligt, M. Bible, B. Natarajan, N.N. Klimov, A.E. Miller, Z. Ahmed, M.R. Hartings, Toward 3D printed hydrogen storage materials made with ABS-MOF composites, Polym. Adv. Technol. 29 (2018) 867-873.

[12] O. Shekhah, J. Liu, R.A. Fischer, C. Woll, MOF thin films: existing and future applications, Chem. Soc. Rev. 40 (2011) 1081-1106.

[13] Y.Y. Zhang, X. Feng, S. Yuan, J.W. Zhou, B. Wang, Challenges and recent advances in MOF-polymer composite membranes for gas separation, Inorg. Chem. Front. 3 (2016) 896-909.

[14] Y.H. Cai, D.Y. Chen, N.J. Li, Q.F. Xu, H. Li, J.H. He, J.M. Lu, Nanofibrous metal-organic framework composite membrane for selective efficient oil/water emulsion separation, J. Membr. Sci. 543 (2017) 10-17.

[15] S. Basu, A. Cano-Odena, I.F.J. Vankelecom, MOF-containing mixed-matrix membranes for CO2/CH4 and CO2/N-2 binary gas mixture separations, Sep. Purif. Technol. 81 (2011) 31-40.

[16] S. Sorribas, B. Zornoza, C. Tellez, J. Coronas, Mixed matrix membranes comprising silica-(ZIF-8) core-shell spheres with ordered meso-microporosity for natural- and bio-gas upgrading, J. Membr. Sci. 452 (2014) 184-192.

[17] Z.N. Shi, C. Xu, F. Chen, Y.X. Wang, L. Li, Q.T. Meng, R. Zhang, Renewable metal-organic-frameworks-coated 3D printing film for removal of malachite green, RSC Adv. 7 (2017) 49947-49952.

[18] Z.Y. Wang, J.J. Wang, M.Y. Li, K.H. Sun, C.J. Liu, Three-dimensional Printed Acrylonitrile Butadiene Styrene Framework Coated with Cu-BTC Metal-organic Frameworks for the Removal of Methylene Blue, Sci. Rep. 4 (2014) 5939.

[19] K.A. Evans, Z.C. Kennedy, B.W. Arey, J.F. Christ, H.T. Schaef, S.K. Nune, R.L. Erikson, Chemically Active, Porous 3D-Printed Thermoplastic Composites, ACS Appl. Mater. Interfaces 10 (2018) 15112-15121.

[20] R. Li, S. Yuan, W. Zhang, H. Zheng, W. Zhu, B. Li, M. Zhou, A. Wing-Keung Law, K. Zhou, 3D Printing of Mixed Matrix Films Based on Metal-Organic Frameworks and Thermoplastic Polyamide 12 by Selective Laser Sintering for Water Applications, ACS Appl. Mater. Interfaces 11 (2019) 40564-40574.

[21] O. Halevi, J.M.R. Tan, P.S. Lee, S. Magdassi, Hydrolytically Stable MOF in 3D-Printed Structures, Adv. Sustain. Syst. 2 (2018) Unsp 1700150.

[22] L. Ge, W. Zhou, A. Du, Z. Zhu, Porous Polyethersulfone-Supported Zeolitic Imidazolate Framework Membranes for Hydrogen Separation, J. Phys. Chem. C. 116 (2012) 13264-13270.

[23] F. Cacho-Bailo, B. Seoane, C. Tellez, J. Coronas, ZIF-8 continuous membrane on porous polysulfone for hydrogen separation, J. Membr. Sci. 464 (2014) 119-126.

[24] D. Nagaraju, D.G. Bhagat, R. Banerjee, U.K. Kharul, In situ growth of metal-organic frameworks on a porous ultrafiltration membrane for gas separation, J. Mater. Chem. A 1 (2013) 8828-8835.

[25] K. Khaletskaya, S. Turner, M. Tu, S. Wannapaiboon, A. Schneemann, R. Meyer, A. Ludwig, G. Van Tendeloo, R.A. Fischer, Self-Directed Localization of ZIF-8 Thin Film Formation by Conversion of ZnO Nanolayers, Adv. Funct. Mater. 24 (2014) 4804-4811.

[26] M. Weber, A. Julbe, A. Ayral, P. Miele, M. Bechelany, Atomic Layer Deposition for Membranes: Basics, Challenges, and Opportunities, Chem. Mat. 30 (2018) 7368-7390.

[27] C. Marichy, M. Bechelany, N. Pinna, Atomic Layer Deposition of Nanostructured Materials for Energy and Environmental Applications, Adv. Mater. 24 (2012) 1017-1032.

[28] T. Tynell, M. Karppinen, Atomic layer deposition of ZnO: a review, Semicond. Sci. Technol. 29 (2014) 043001.

[29] V. Miikkulainen, M. Leskela, M. Ritala, R.L. Puurunen, Crystallinity of inorganic films grown by atomic layer deposition: Overview and general trends, J. Appl. Phys. 113 (2013) 021301.

[30] J.J. Zhao, M.D. Losego, P.C. Lemaire, P.S. Williams, B. Gong, S.E. Atanasov, T.M. Blevins, C.J. Oldham, H.J. Walls, S.D. Shepherd, M.A. Browe, G.W. Peterson, G.N. Parsons, Highly Adsorptive, MOF-Functionalized Nonwoven Fiber Mats for Hazardous Gas Capture Enabled by Atomic Layer Deposition, Adv. Mater. Interfaces 1 (2014) 1400040.

[31] J.J. Zhao, B. Gong, W.T. Nunn, P.C. Lemaire, E.C. Stevens, F.I. Sidi, P.S. Williams, C.J. Oldham, H.J. Walls, S.D. Shepherd, M.A. Browe, G.W. Peterson, M.D. Losego, G.N. Parsons,

Conformal and highly adsorptive metal-organic framework thin films via layer-by-layer growth on ALD-coated fiber mats, J. Mater. Chem. A 3 (2015) 1458-1464.

[32] D.T. Lee, J.J. Zhao, C.J. Oldham, G.W. Peterson, G.N. Parsons, UiO-66-NH2 Metal Organic Framework (MOF) Nucleation on TiO2, ZnO, and Al2O3 Atomic Layer Deposition-Treated Polymer Fibers: Role of Metal Oxide on MOF Growth and Catalytic Hydrolysis of Chemical Warfare Agent Simulants, ACS Appl. Mater. Interfaces 9 (2017) 44847-44855.

[33] M. Bechelany, M. Drobek, C. Vallicari, A. Abou Chaaya, A. Julbe, P. Miele, Highly crystalline MOF-based materials grown on electrospun nanofibers, Nanoscale 7 (2015) 5794-5802.

[34] M. Drobek, M. Bechelany, C. Vallicari, A. Abou Chaaya, C. Charmette, C. Salvador-Levehang, P. Miele, A. Julbe, An innovative approach for the preparation of confined ZIF-8 membranes by conversion of ZnO ALD layers, J. Membr. Sci. 475 (2015) 39-46.

[35] Q. Zheng, Y.C. Fu, J.Q. Xu, Advances in the Chemical Sensors for the Detection of DMMP - A Simulant for Nerve Agent Sarin, in: M. Li, D. Yu (Eds.) 2010 Symposium on Security Detection and Information Processing, Elsevier Science Bv, Amsterdam, 2010, pp. 179-184.

[36] C. Montoro, F. Linares, E.Q. Procopio, I. Senkovska, S. Kaskel, S. Galli, N. Masciocchi, E. Barea, J.A.R. Navarro, Capture of Nerve Agents and Mustard Gas Analogues by Hydrophobic Robust MOF-5 Type Metal-Organic Frameworks, J. Am. Chem. Soc. 133 (2011) 11888-11891.

[37] S.Y. Moon, Y.Y. Liu, J.T. Hupp, O.K. Farha, Instantaneous Hydrolysis of Nerve-Agent Simulants with a Six-Connected Zirconium-Based Metal-Organic Framework, Angew. Chem.-Int. Edit. 54 (2015) 6795-6799.

[38] Y.Y. Liu, A.J. Howarth, N.A. Vermeulen, S.Y. Moon, J.T. Hupp, O.K. Farha, Catalytic degradation of chemical warfare agents and their simulants by metal-organic frameworks, Coord. Chem. Rev. 346 (2017) 101-111.

[39] D. Troya, Reaction Mechanism of Nerve-Agent Decomposition with Zr-Based Metal Organic Frameworks, J. Phys. Chem. C 120 (2016) 29312-29323.

[40] X.J. Ma, Y.T. Chai, P. Li, B. Wang, Metal-Organic Framework Films and Their Potential Applications in Environmental Pollution Control, Accounts Chem. Res. 52 (2019) 1461-1470.

[41] R. Viter, Z. Balevicius, A. Abou Chaaya, I. Baleviciute, S. Tumenas, L. Mikoliunaite, A. Ramanavicius, Z. Gertnere, A. Zalesska, V. Vataman, V. Smyntyna, D. Erts, P. Miele, M. Bechelany, The influence of localized plasmons on the optical properties of Au/ZnO nanostructures, J. Mater. Chem. C 3 (2015) 6815-6821.

[42] F. Almazan, I. Pellejero, A. Morales, M.A. Urbiztondo, J. Sese, M.P. Pina, J. Santamaria, Zeolite based microconcentrators for volatile organic compounds sensing at trace-level: fabrication and performance, J. Micromech. Microeng. 26 (2016) 084010.

[43] REHAU. Acrylonitrile-butadiene-styrene (RAU-ABS) MATERIAL DATA SHEET AV0270 EN.

[44] M. Drobek, J.H. Kim, M. Bechelany, C. Vallicari, A. Julbe, S.S. Kim, MOF-Based Membrane Encapsulated ZnO Nanowires for Enhanced Gas Sensor Selectivity, ACS Appl. Mater. Interfaces 8 (2016) 8323-8328.

[45] M. Weber, J.H. Kim, J.H. Lee, J.Y. Kim, I. Iatsunskyi, E. Coy, M. Drobek, A. Julbe, M. Bechelany, S.S. Kim, High-Performance Nanowire Hydrogen Sensors by Exploiting the Synergistic Effect of Pd Nanoparticles and Metal-Organic Framework Membranes, ACS Appl. Mater. Interfaces 10 (2018) 34765-34773.

[46] J. Iqbal, A. Jilani, P.M. Ziaul Hassan, S. Rafique, R. Jafer, A.A. Alghamdi, ALD grown nanostructured ZnO thin films: Effect of substrate temperature on thickness and energy band gap, J. King Saud Univ. Sci. 28 (2016) 347-354.

[47] R. Viter, I. Iatsunskyi, V. Fedorenko, S. Tumenas, Z. Balevicius, A. Ramanavicius, S. Balme, M. Kempinski, G. Nowaczyk, S. Jurga, M. Bechelany, Enhancement of Electronic and Optical Properties of ZnO/Al2O3 Nanolaminate Coated Electrospun Nanofibers, J. Phys. Chem. C 120 (2016) 5124-5132.

[48] O. Karagiaridi, M.B. Lalonde, W. Bury, A.A. Sarjeant, O.K. Farha, J.T. Hupp, Opening ZIF-8: A Catalytically Active Zeolitic Imidazolate Framework of Sodalite Topology with Unsubstituted Linkers, J. Am. Chem. Soc. 134 (2012) 18790-18796.

[49] F. Puype, J. Samsonek, J. Knoop, M. Egelkraut-Holtus, M. Ortlieb, Evidence of waste electrical and electronic equipment (WEEE) relevant substances in polymeric food-contact articles sold on the European market, Food Addit. Contam. Part A-Chem. 32 (2015) 410-426.

[50] N.T. Thanh Truc, B.K. Lee, Selective separation of ABS/PC containing BFRs from ABSs mixture of WEEE by developing hydrophilicity with ZnO coating under microwave treatment, J. Hazard. Mater. 329 (2017) 84-91.

[51] J. Cravillon, S. Munzer, S.J. Lohmeier, A. Feldhoff, K. Huber, M. Wiebcke, Rapid Room-Temperature Synthesis and Characterization of Nanocrystals of a Prototypical Zeolitic Imidazolate Framework, Chem. Mat. 21 (2009) 1410-1412.

[52] A. Anzlovar, Z.C. Orel, K. Kogej, M. Zigon, Polyol-Mediated Synthesis of Zinc Oxide Nanorods and Nanocomposites with Poly(methyl methacrylate), J. Nanomater. (2012) 760872.

[53] D.W. Dong, S. Tasaka, S. Aikawa, S. Kamiya, N. Inagaki, Y. Inoue, Thermal degradation of acrylonitrile-butadiene-styrene terpolymer in bean oil, Polym. Degrad. Stabil. 73 (2001) 319-326.

[54] S.Y. Yang, J.R. Castilleja, E.V. Barrera, K. Lozano, Thermal analysis of an acrylonitrile-butadiene-styrene/SWNT composite, Polym. Degrad. Stabil. 83 (2004) 383-388.

[55] S. Wojtyla, P. Klama, T. Baran, Is 3D printing safe? Analysis of the thermal treatment of thermoplastics: ABS, PLA, PET, and nylon, J. Occup. Environ. Hyg. 14 (2017) D80-D85.

[56] P. Krokidas, M. Castier, S. Moncho, E. Brothers, I.G. Economou, Molecular Simulation Studies of the Diffusion of Methane, Ethane, Propane, and Propylene in ZIF-8, J. Phys. Chem. C. 119 (2015) 27028-27037.

[57] S.M. Kanan, A. Waghe, B.L. Jensen, C.P. Tripp, Dual WO3 based sensors to selectively detect DMMP in the presence of alcohols, Talanta 72 (2007) 401-407.

[58] D.A. Panayotov, J.R. Morris, Uptake of a Chemical Warfare Agent Simulant (DMMP) on TiO2: Reactive Adsorption and Active Site Poisoning, Langmuir 25 (2009) 3652-3658.

[59] A.R. Head, R. Tsyshevsky, L. Trotochaud, Y. Yu, O. Karslioglu, B. Eichhorn, M.M. Kuklja, H. Bluhm, Dimethyl methylphosphonate adsorption and decomposition on MoO2 as studied by ambient pressure x-ray photoelectron spectroscopy and DFT calculations, J. Phys.-Condes. Matter 30 (2018) 134005.

[60] G.Y. Liu, L.Y. Li, X.D. Huang, S.N. Zheng, X.M. Xu, Z.X. Liu, Y.G. Zhang, J. Wang, H. Lin, D.H. Xu, Adsorption and removal of organophosphorus pesticides from environmental water and soil samples by using magnetic multi-walled carbon nanotubes @ organic framework ZIF-8, J. Mater. Sci. 53 (2018) 10772-10783.

[61] Y. Zhou, L. Zhou, X.H. Zhang, Y.L. Chen, Preparation of zeolitic imidazolate framework-8 /graphene oxide composites with enhanced VOCs adsorption capacity, Micropor. Mesopor. Mat. 225 (2016) 488-493.

[62] K. Huynh, S. Holdren, J.K. Hu, L.N. Wang, M.R. Zachariah, B.W. Eichhorn, Dimethyl Methylphosphonate Adsorption Capacities and Desorption Energies on Ordered Mesoporous Carbons, ACS Appl. Mater. Interfaces 9 (2017) 40638-40644.